International Journal of Computer Information Systems and Industrial Management Applications
ISSN 2150-7988 Volume 18(20s) 2026 pp. 603-616
https://doi.org/10.70917/ijcisim-2026-5202
Article

Analytical Model for the n-Channel MOSFET's Surface Potential Considering QM Effects in Valence and Conduction Band

K V Jyothi Prakash[1], G S Jayadeva[2]

[1]Department of Electronics and Communication Engineering, Siddaganga Institute of Technolgy, Tumkur, Karnataka-572103, India.
Email: jyothiprakashkv@sit.ac.in
[2]Department of Electronics and Communication Engineering, BMS Institute of Technology and Management, Bangalore, Karnataka – 560064, India.
Email: jayadevags@gmail.com

Abstract: Incorporating quantum mechanical (QM) effects into nMOSFETs with a 100 Si surface orientation is suggested in this work through a physics-based analytical model that takes into account the triangular potential well approximation in the valence and conduction bands. The model's surface potential is valid for a large range of device parameters, is continuous, and smooth from the accumulation area to the strong inversion region; it also does not need fitting parameters or smoothing functions. These model's C_G versus V_GB properties, as well as the surface potential, electron density, and hole density in their respective operating zones, agree extremely well with the published findings of self-consistent solutions to the Schrödinger and Poisson equations. There is a strong agreement between the numerically acquired data from the generated implicit expression and the surface potential values calculated using the simplified analytical model and its derivative.
Keywords: Surface potential,QM-effects, analytical model, triangular potential well, valence and conduction band, nMOSFET

1. INTRODUCTION

In current generation sub-100 nm MOSFETs, quantum confinement is a consequence of the extraordinarily strong electric field at the oxide semiconductor interface caused by the very thin gate oxide and very high channel doping. In order to correctly understand the physical device features and model the devices, QM effects become very critical for both the inversion [1]-[8] and accumulation area [5]-[11]. This is because the usual classical theory is inadequate for these devices. Research demonstrating the development of analytical models from a compact modelling approach that include QM effects in the inversion area has been extensively documented [8], [12]-[17].

Realistic data simulation for modern devices in VLSI and ULSI applications, accurate interpretation of experimental data, and capacitance-voltage and current-voltage measurements of sub-100 nm MOSFETs all depend on an accurate model of the accumulation area [8, 11, 18, 19]. For the purpose of simulating the electrical performance of floating-gate EEPROM cells [9], [18]-[20], and in varactor-based circuits like voltage controlled oscillators [21], it is crucial to analyse quantum confinement in the accumulation layer in order to account for source/drain overlapped region resistances and tunnel injection of charge carriers.

Quantum confinement is shown in the accumulation area at low temperatures [22], [23] and at room temperature or higher temperatures [4, 18, 19]. The creation of a potential well at the surface can occur even in the absence of an external field, as demonstrated by Baraff and Joel [23]. Lower subband energies will be significantly occupied for

bigger electric fields at the oxide semiconductor interface higher than 30 MV/m, as later proved by Moglestue [24]. The quantisation effect is also present in weak accumulation, as shown by Pacelli et al. [25].

While the analysis in the accumulation region is more complicated from a physics perspective owing to the distribution of carriers in both bound energy levels and the continuous energy spectrum, it is still possible to obtain an analytical solution by approximating this region using a triangle potential well [6, 8]. On the other hand, from a compact modelling standpoint, including QM effects in the accumulation area receives surprisingly little attention [6, 8, 10, 26].

In the accumulation area, capacitance and surface potential values derived classically vary from those determined quantum mechanically by repeatedly solving the Poisson and Schrödinger equations (Villanueva et al., [26]). By numerically obtaining the carrier sheet density and surface potential using the triangular potential well approximation, Yutao Ma et al. [6] demonstrated the validity of this approach in both the inversion and accumulation regions, as compared to the values obtained by solving the Schrödinger and Poisson equations in a self-consistent manner. It is computationally costly, as pointed out by [28]-[30], but Marin et al. [27] was able to derive the surface potential and charge distribution for asymmetric UTB MOSFETs by solving the Schrödinger and Poisson equations in a triangular quantum well.

The surface potential in the accumulation and inversion area was computed by Pregaldiny et al. [8] taking QM effects into account. There are a number of problems with this computation, including the fact that it does not produce accurate surface potential values close to the flat band [16]. A QM adjustment to the classical surface potential is included in the other models that are based on surface potentials [7], [21], [31]-[35]. Some of these models employ fitting parameters; for example, [7], [31]–[33] make use of the van Dort band gap widening technique [36], [21], [34] make use of the QM charge sheet model, and [35] incorporates QM effects by using the effective oxide thickness. In [16], an analytical model that is better grounded in physics and runs continuously from accumulation to strong inversion areas is suggested, with QM effects being taken into account just in the inversion region. Therefore, it is possible to create a simpler analytical model to calculate the surface potential that takes into consideration the effects of QM in the accumulation and inversion regions, guaranteeing a smooth transition from the accumulation to the strong inversion operating regions.

The goal of this study is to include QM effects in the valence band of the framework, which previously only included QM effects in the conduction band [16], using computationally efficient simplified analytical expressions that guarantee a smooth transition from the accumulation to the strong inversion region of operation. The first step in arriving at the surface potential expression is to derive an implicit expression from the 1-D Poisson equation that takes QM effects into account. Then, with the use of elementary mathematical tools, we can derive an exact closed-form expression for the surface potential; this expression does not need smoothing functions, and it provides computing efficiency, continuity from the accumulation area to the strong inversion region, and so on. Section II delves into the explanation of the implicit equation for the surface potential, while Section III lays out the analytical approach. The validity of the findings acquired from the presented data and numerical techniques with the results produced from the suggested analytical model is described in Section IV. Section V offers the final verdict.

2. MODEL

Using QM effects in the valence and conduction bands, this study aims to generate a single surface potential expression that is valid in all three operating zones of nMOSFETs. To do this, we first find the surface potential expression in terms of the accumulation and inversion charges per unit area, as well as the applied gate voltage, using the 1-D Poisson equation. Using the triangular potential well approximation in the channel, the formulas for Q_a and Q_i as functions of surface potential (□_s) and applied gate voltage V_GB are found for nMOSFETs with a 100° Si surface orientation. Through the resolution of these equations, a surface potential implicit expression that takes into account QM confinement in the valence and conduction bands, omitting the Q_a and Q_i factors, may be derived.

But solving the resulting formula numerically is the sole option, and it's a computationally intensive process. An analytical approximation of this statement is developed to make it acceptable for compact models. Then, the Newton Raphson method's correction stages are applied to provide a more precise estimate of the surface potential. Taking into account the structure as a metal, an insulator, or a semiconductor, the following subsections provide a full explanation of the aforementioned technique. We follow the notations of that study for continuity, as the formula for the inversion layer charge is previously stated in [16], therefore our focus here is on obtaining an expression for hole charge.

2.1 Surface potential as a function of and using 1-D Poisson equation $(\psi_s) Q_a, Q_i V_{GB}$

Using the one-dimensional Poisson equation, we can get the electrostatic potential energy from the Si-SiO2 interface to the bulk by

$$\frac{d^2\psi}{dx^2} = \frac{-q\left(n_{po} - p_{po} + p_p - n_p\right)}{\varepsilon_{si}} (1)$$

where ψ stands for the electrostatic potential, n_p and p_p denote the electron and hole concentrations, and n_{po} and p_{po}, respectively, denote the equilibrium electron and hole concentrations in the bulk for a p-type substrate under charge neutrality conditions. In the accumulation and inversion regions of operation, the concentrations of holes and electrons are large, respectively. From say at $x = x_a$ by holes and at $x = x_i$ these regions to the oxide semiconductor interface, where the electric field (E) and potential (P) are zero, the concentrations of these particles are constrained to a small distance. We can determine that, at the oxide-semiconductor interface, where $\psi = \psi_s$ and $E = E_s$, in the respective accumulation and inversion regions of operation, the confinement takes place in a very thin layer assuming sheet charge density. Taking into account that $x_a \approx x_i$ and integrating (1) from the confinement distance to $x = 0$ yields this result.

$$\frac{1}{2}E_s^2 = \left[\frac{-qn_{po}\psi}{\epsilon_{si}} + \frac{qp_{po}\psi}{\epsilon_{si}}\right]_0^{\psi_s} - \frac{q}{\epsilon_{si}}\int_{x_a}^{0} p_p \frac{d\psi}{dx}dx + \frac{q}{\epsilon_{si}}\int_{x_i}^{0} n_p \frac{d\psi}{dx}dx. \quad (2)$$

For inversion, the electric field strength $d\psi/dx$, and (E_s) for the accumulation zone of operation, $E_s = -Q_s/\epsilon_{si}$, where Q_s is the total semiconductor charge per unit area, reaches a maximum (E_s) at the oxide semiconductor interface in equation (2) before progressively decreasing to zero in the bulk. The charge per unit area of the hole (Q_a) and the electron (Q_i) may be written as Q_a=- $q\int$ _(x_a)^0 〖$p\_p\ dx$〗 and $Q\_i = -q\int$ _(x_i)^0▒ 〖$n\_p\ dx$〗, respectively, if the charge confinement distance is very narrow in the area of operation in question. At x=0 in the accumulation layer and -$E\_s - (Q\_a\ /\ (\epsilon\_si))\ at\ x = x\_a$, the electric field is 〖$-E$〗 _s. In the inversion layer, it is E_s at $x = 0$ and $E\_s + ((Q\_i)\ /\ \epsilon\_si))$ at $x = x\_i$. The average electric field in the accumulation layer is thus given by and in the inversion layer by

$$E_{effa} = -E_s - \frac{Q_a}{2\epsilon_{si}} = \frac{-Q_s}{\epsilon_{si}}\left(1 + \frac{Q_a}{2Q_s}\right) \quad (3a)$$

$$E_{eff} = E_s + \frac{Q_i}{2\epsilon_{si}} = \frac{-Q_s}{\epsilon_{si}}\left(1 - \frac{Q_i}{2Q_s}\right). \quad (3b)$$

Because we're assuming that $d\psi/dx$ is constant, equal to E_{effa} in the accumulation layer and E_{eff} inside the inversion layer causes the triangle potential well in the corresponding operational area, (2) may be reduced to

$$\frac{1}{2}E_s^2 = \frac{-q}{\epsilon_{si}}\left[n_{po}\psi_s - p_{po}\psi_s\right] - \frac{Q_a}{\epsilon_{si}}\left[E_s + \frac{Q_a}{2\epsilon_{si}}\right] - \frac{Q_i}{\epsilon_{si}}\left[E_s + \frac{Q_i}{2\epsilon_{si}}\right] \quad (4)$$

solving the quadratic equation (4) for E_s

$$E_s = -\left(\frac{Q_a + Q_i}{\epsilon_{si}}\right) \pm \sqrt{\frac{2}{\epsilon_{si}}\left[\frac{Q_a Q_i}{\epsilon_{si}} - q\left(n_{po}\,\psi_s - p_{po}\,\psi_s\right)\right]}. \quad (5)$$

In (5), "+" sign is applicable for positive ψ_s and "" sign is applicable for negative ψ_s, ionised impurities in the inversion layer are disregarded in the derivation of (5) and in the above and below flat band operation areas, respectively [16].

Now that we have Gauss law, we may express it as

$$Q_s = \epsilon_{si} E_s = C_{ox}\left(V_{GB} - V_{FB} - \psi_s\right). \quad (6)$$

From equation (5) and (6) we can write

$$C_{ox}\left(V_{GB} - V_{FB} - \psi_s\right) = -(Q_a + Q_i) \pm \epsilon_{si}\sqrt{\frac{2}{\epsilon_{si}}\left[\frac{Q_a Q_i}{\epsilon_{si}} + q p_{po}\,\psi_s\left(1 - \frac{n_{po}}{p_{po}}\right)\right]}. \quad (7)$$

Considering $p_{po} = N_A$ and the electron quasi Fermi potential (ξ) in a MOSFET channel is equal to channel to bulk potential $V_{CB}(y)$, which varies from source-to-bulk voltage (V_{SB}) to drain-to-bulk voltage (V_{DB}), at the source and drain end respectively, (7) can be written as

$$V_{GB} - V_{FB} - \psi_s = -\left(\frac{Q_a + Q_i}{C_{ox}}\right) \pm \gamma\sqrt{\frac{Q_a Q_i}{q\epsilon_{si} N_A} + \psi_s(1 - e^{-\emptyset_n/V_t})}. \quad (8)$$

All areas of operation have a very tiny accumulation and inversion charge product term (< 10-10) under the square root (8), since the charge components are negligibly small at any point of operation relative to the other charge terms. It is entirely disregarded and has no bearing on the surface potential computation; hence, equation (8) reduces to

$$V_{GB} - V_{FB} - \psi_s = -\left(\frac{Q_a + Q_i}{C_{ox}}\right) \pm \gamma\sqrt{\psi_s(1 - e^{-\emptyset_n/V_t})} \quad (9)$$

where $\gamma = \sqrt{2\epsilon_{si} q N_A}/C_{ox}$ is the body effect parameter and $\emptyset_n = 2\emptyset_B + \xi$, $\emptyset_B = V_t \ln(N_A/n_i)$stands for the Fermi potential. In the subthreshold area mentioned before, where the buildup charge(Q_a) is neglected, (9) deduces, without the variables for accumulating charge, the surface potential equation (8) from [16]. When the charges of electrons and holes are predominant in the inversion and accumulation areas of operation, equation (9) may be reduced as$C_{ox}\left(V_{GB} - V_{FB} - \psi_s\right) \approx -Q_i$, $C_{ox}\left(V_{GB} - V_{FB} - \psi_s\right) \approx -Q_a$that is, in turn. The QM effects are negligible in the weak inversion or depletion area because of the high subband occupancy [7], [37].

2.2 Accumulation and Inversion Layer Charge Density Considering QM Effects

In order to determine the charge density of the accumulation and inversion layers, this model suggests using nMOSFETs with a 100 degree Si surface orientation. The method for calculating the charge density of the accumulation layer is detailed in the paragraph that follows. This model makes use of the data obtained from the method for calculating the inversion layer charge density, which is detailed in [16].

Because of the complexity of the valence band structure—which must account for the majority of carriers from both the bulk of the semiconductor and the quantised energy levels at the Si-SiO2 interface—theoretical treatment of the valence band is more difficult than conduction band treatment [5, 8, 19]. On the other hand, triangular potential well approximation has been shown to be useful for precise accumulation layer analysis [8, 25, 26]. The valleys are partitioned into two subbands (ladders) in the effective mass approximation, and each subband has a degeneracy factor of one. A large hole's longitudinal effective mass is present in the bottom subband, which is the unprimed ladder$m_{zLa} = 0.5\, m_0$, light-hole transverse effective mass is present in the primed ladder, a higher collection of

subbands$m_{zHa} = 0.16\ m_0$[5]. With the suffixes L and H, respectively, these lower and higher subband energy levels are shown in Fig. 1.

[Image could not be embedded — unsupported format]

Fig. 1. Energy band diagram of metal/SiO2/p-Si structure showing four lowest subbands in accumulation region.

The charge density in the accumulation layer may be calculated with QM effects taken into consideration using the triangular potential well approximation [11], as

$$Q_a = \sum_i A_{ia} \sum_j \ln\left(1 + \exp\left(\frac{E_{Fp} - E_{ija}}{kT}\right)\right)_{i=L,H\ j=0,1,2\ldots} \quad (10)$$

where E_{Fp} is the hole quasi Fermi energy with respect to the top of valence band at Si-SiO2 interface as shown in Fig. 1. $A_{ia} = (qn_{via}m_{dia}kT)/(\pi\hbar^2)$ is a constant for a particular valley, $\hbar$ is the reduced Planck's constant, m_{dia}has the same value as the density of states' effective mass per valley for holes, which is$0.5\ m_0$ and $0.16\ m_0$ for lower (m_{dLa}) and higher (m_{dHa}) valleys respectively, $n_{via} = 1$ for both valleys, as the energy subband in accumulation is not degenerate, and$E_{ija}$is the potential energy that matches thej^{th} subband of the i^{th} valley [4], [6], given as

$$E_{ija} = \left(\frac{\hbar^2}{2m_{zia}}\right)^{1/3} \left[\left(\frac{3\pi q}{2}\right) E_{effa}(j + 3/4)\right]^{2/3}_{i=L,H\ \ j=0,1,2\ldots} \quad (11)$$

where m_{zia} is the accumulation layer quantization effective mass, E_{effa} is the effective electric field, expressed as

$$E_{effa} = -Q_s/\eta\epsilon_{si}. \quad (12)$$

In order to simplify things even further and avoid implicitly calculating Q_a., (12) is used in (11) instead of (3a). The subbands near the top of the valence band, where the electric field which is very close to E_s will have higher charge concentration and play an important role. The results obtained from suggested model using the aforesaid approximations,$\eta = 1.3$ exhibits good fit with the self-consistent solution of Schrödinger and Poisson equations, with ,$\eta = 1.3$ and is utilised as a constant. The expected difference between the inversion layer and this section is that the value of η is 1.1 [16], but the values used here are slightly different from [6]. We obtain by inserting (12) and (6) into equation (11):

$$E_{ija} = \left(\frac{\hbar^2}{2m_{zia}}\right)^{1/3} \left[\left(\frac{3\pi q}{2}\right)\left(\frac{-C_{ox}\left(V_{GB} - V_{FB} - \psi_s\right)}{\eta\,\epsilon_{si}}\right)(j + 3/4)\right]^{2/3}_{i=L,H\ \ j=0,1,2\ldots} \quad (13)$$

From Fig. 1, ψ_s can be written as

$$-\psi_s = (E_{FP}/q) + (E_g/2q) - \emptyset_B + \xi. \quad (14)$$

In (14), $\psi_s$meaning it's negative because, in this case, the energy bands are bending downwards relative to the reference point, rather than upwards, as they are in an inversion. Using insteadE_{FP} from equation (14) in (10), the expression for accumulation charge density Q_a can be obtained as

$$Q_a = \sum_i A_{ia} \sum_j \ln\left[1 + \exp\left(\frac{-\psi_s - E_g/2q + \emptyset_B - \xi - E_{ija}/q}{V_t}\right)\right]_{i=L,H\ \ j=0,1,2\ldots} \quad (15)$$

Now substituting Q_a from (15) and Q_iEquation (9) integrates QM effects in the valence and conduction bands, and the implicit expression of the surface potential, which is continuous from the accumulation zone to the strong inversion region, is derived from equation (14) of [16].

2.3 Normalisation and Conditioning

After normalising Equation (9) to make all variables dimensionalless quantities, we get

$$U_{GFB} - u_s = -(q_{an} - q_n) \pm \gamma_1\sqrt{u_s(1 - e^{-u_n})} \qquad (16)$$

where $U_{GFB} = (V_{GB} - V_{FB})/V_t$, $u_s = \psi_s/V_t$, $\gamma_1 = \gamma/\sqrt{V_t}$, $u_n = \emptyset_n/V_t$

from (15)

$$q_{an} = \frac{Q_a}{V_t C_{ox}} = \sum_i a_{ina} \sum_j \ln[1 + e^{-u_s - u_{ua} - e_{ija}}]_{i=L,H \;\; j=0,1,2\ldots} \qquad (17)$$

where $a_{ina} = (A_{ia}/C_{ox}V_t) = (q^2 n_{via} m_{dia})/(\pi\hbar^2 C_{ox})$, $u_{ua} = ((E_g/2q) - \emptyset_B + \xi)/V_t$

$$e_{ija} = \frac{E_{ija}}{qV_t} = \left(\frac{\hbar^2}{2m_{zia}qV_t}\right)^{1/3} \left[\left(\frac{3\pi C_{ox}}{2\eta\epsilon_{si}}\right)(-(U_{GFB} - u_s))(j + 3/4)\right]^{2/3}_{i=L,H \;\; j=0,1,2\ldots} \qquad (18)$$

Equations (17) and (18b) of [16] provide the expressions for energy levels and normalised inversion layer charge density, respectively.

All operating zones are well-served by the surface potential expression (16), with the exception of the flat band.($U_{GFB} = 0$), when mathematical conditioning is necessary. Otherwise, surface potential based compact models have difficulties when calculating from the accumulation zone to the strong inversion or vice versa [38]. For equation (16), at the flat band point, $U_{GFB} = u_s = 0$, $e_{ij} = 0$, $e_{ija} = 0$, except q_n, q_{an}whereas the phrase is defined as square root. Terms' conditioning subject to square root and$q_n$is handled in accordance with the explanation provided in [16], and the equation (16) is replaced with as

$$U_{GFB} - u_s = -(q_{an} - q_n) \pm \gamma_1\sqrt{u_s}. \qquad (19)$$

Now to condition accumulation layer charge $q_{an} = 0$ at flat band, (17) is modified as

$$q_{an} = \sum_i a_{ina} \sum_j \ln[1 + e^{-u_s - u_{ua} - e_{ija}} - e^{-u_{uae}}]_{i=L,H \;\; j=0,1,2\ldots} \qquad (20)$$

where $e^{-u_{uae}}$ is added in (20) instead of $e^{-u_{ua}}$, since u_{ua} is not very large quantity and the term $e^{-u_{ua}}$ cannot be neglected as it is. If neglected it affects specifically the surface potential and charge density in depletion region. Hence the term u_{ua} is modified to depend on electric field, based on van Dort model [36], as

$$u_{uae} = ((E_g/2q) - (1 - \Delta_\epsilon)\emptyset_B + \xi)/V_t. \qquad (21)$$

In other cases, the surface potential will be negligible, but at the flat band it will be zero. The idea of$\Delta_\epsilon =$ $(1/q)[(9\pi\,\hbar q E_f)/(8\sqrt{2m_{zLa}}\,\eta\epsilon_{si})]^{2/3}$ do not contain any fitting parameter, where E_f is the effective electric field and is equal to E_{effa} in accumulation region and E_{eff} in depletion/inversion regions of operation.

2.4 Analytical Approximation for the Surface Potential

When numerically calculated for a given value of, the physics-based, physically consistent, and parameter-free formula (19) yields accurate surface potential values throughout all nMOSFET operating regions.V_{GB}. In order to get the precise value of the continuous surface potential needed in compact models, we will now detail the process of developing an analytical expression as a function of gate voltage. There are three separate areas of activity that we take into account for this: (i) the accumulation region, where$U_{GFB} \leq 0$, (ii) depletion region where $0 < U_{GFB} < U^*_{GFB}$, and (iii) inversion region where $U_{GFB} \geq U^*_{GFB}$. Here $U^*_{GFB}$is predicted to happen at a certain point, and the assumption is made that the concentration of electrons and holes is negligibly tiny in comparison to the concentration of depletion

charges.$u_s = u_u = ((E_g/2q) + \emptyset_B + \xi)/V_t$, which implies that the strong inversion occurs at $\psi_s = (E_g/2q) + \emptyset_B + \xi$, which is slightly greater than $\psi_s = 2\emptyset_B + \xi$ taken in classical models as expected. Now, defining $U_{GFB} = U^*_{GFB}$ when $u_s = u_u$, from (19), we get

$$U^*_{GFB} = u_u + \gamma_1\sqrt{u_u}. \quad (22)$$

A change in threshold voltage as a result of quantum mechanical processes, doping concentration, or applied drain voltage is intrinsically taken into consideration in Equation (22).

In the first phase, we derive three distinct analytical expressions by properly approximating (18b) of [16], (19), and (20) to acquire a relatively accurate value of the surface potential.(u_{s1}), for various operational areas. A correction term is necessary to get a surface potential value that is precise enough$r(u_{s1}, U_{GFB})$, obtained using Newton Raphson expansion [39], [40], is added

$$u_s = u_{s1} + r(u_{s1}, U_{GFB}). \quad (23)$$

If you want your surface potential to be more precise, you may perform the correction step again.(u_s)in sophisticated models. Below is a detailed description of the technique that may be followed to acquire an analytical equation for us.

2.5 1) Step-1: First Approximation

Just as previously stated, the next sections provide the approximate equation for the surface potential 〖(u〗_s1) for the accumulation, depletion, and inversion zones of operation.

2.6 a) Accumulation region($U_{GFB} \leq 0$)

When we only take into account the hole charge component in equation (19), we find that the contributions of depletion and inversion layer charges are so insignificant that they are not even noticeable in the accumulation region of operation.

$$U_{GFB} = -q_{an}. \quad (24)$$

Despite the fact that a highly accurate surface potential value requires considering a huge number of subbands in the valence and conduction bands. It is enough to get a rough estimate of the surface potential in the first approximation, however.(u_{s1}), think about only the lowest energy subband in the lower valley and just replacing$u_s = u_a$ in the accumulation charge term in (24) and simplifying

$$u_a = -u_{ua} - e^{u_{ua}}_{L0a} - \ln[e^{-Z} + e^{-u_{uae}} - 1] \quad (25)$$

where $Z = U_{GFB}/a_{Lna}$. The accuracy attained using (25) is adequate in accumulation area, yet in the accumulation to depletion transition region, the linear termu_s in (19) and the accumulating term are similar.(q_{an}). Hence to lessen the inaccuracy in the transition region, substitutingu_s by u_a in both linear and depletion terms, and substituting$u_s = u_{s1}$ in accumulation charge density term in (19), we get

$$u_{s1} = -u_{ua} - e^{u_{ua}}_{L0a} - \ln[e^{Z_a} + e^{-u_{uae}} - 1] \quad (26)$$

where $Z_a = (-U_{GFB} + u_a - \gamma_1\sqrt{u_a})/a_{Lna}$.

2.7 b) Depletion region($0 < U_{GFB} < U^*_{GFB}$)

An approximation of the surface potential is obtained by using the simplification method borrowed from [16] and ignoring the roles played by electron and hole charges in (19).

$$u_{s1} = \frac{k_1 - \sqrt{{k_1}^2 - 4k_2}}{2} \quad (27)$$

where $k_1 = 2(U_{GFB} + q_t) + {\gamma_1}^2,\ k_2 = (U_{GFB} + q_t)^2, q_t = q_{an}^{L0} - q_n^{L0}, q_n^{L0} = a_L \ln\left[1 + e^{u_d - u_u - e_{L0}^{u_d}} - e^{-u_u}\right]$

$q_{an}^{L0} = a_{Lna} \ln\left[1 + e^{-u_d - u_{ua} - e_{L0a}^{u_d}} - e^{-u_{uae}}\right]$ and

$u_d = 0.5\left[2U_{GFB} + {\gamma_1}^2 - \gamma_1\sqrt{4U_{GFB} + {\gamma_1}^2}\right]$. The equations q_n^{L0} and $q_{an}^{L0}$are acquired by focusing just on the lowest subband from equation (18b) in references [16] and (20). Two of the equations in the referenced work, (26) and (27) are identical in form. Having said that, the cumulative term ink_1 and $k_2$are now altered since the accumulation region's quantum confinement is being considered. It makes no difference whether the accumulation terms are calculated classically or quantum mechanically; in the depletion region of operation, their contribution is tiny and insignificant.

2.8 c) Inversion region($U_{GFB} \geq U_{GFB}^*$)

Since the contributions of the accumulation and depletion layers are negligible in the inversion zone of operation, we may isolate the electron charge component in equation (19) and get

$$U_{GFB} = q_n. \qquad (28)$$

To simplify the formula for the surface potential (u_s1) in the accumulation area, we may use the electron charge in the lowest subband of the lower valley and replace u_s=u_i in the inversion charge term (q_n) in equation (28) as previously mentioned.

$$u_i = u_u + e_{L0}^{u_u} + \ln[e^{Z_1} + e^{-u_u} - 1] \qquad (29)$$

where $Z_1 = U_{GFB}/a_L$. Within the area spanning the transition from depletion to inversion, the precision attained using equation (29) is adequate, with the exception of the linear factoru_s in (19) is comparable with the inversion term (q_n). Hence to obtain smooth transition from depletion to inversion region, replacing u_s by u_i in both linear and depletion terms, and substituting $u_s = u_{s1}$ in inversion charge density term in (19), we get the approximate value of surface potential in the inversion region as

$$u_{s1} = u_u + e_{L0}^{u_u} + \ln[e^{Z_i} + e^{-u_u} - 1) \qquad (30)$$

where $Z_i = (U_{GFB} - u_i - \gamma_1\sqrt{u_i})/a_L$.

2.9 2) Step-2: Accurate surface potential with higher order correction

The initial approximations of the surface potential in the accumulation, depletion, and inversion areas, as determined by equations (26), (27), and (30), respectively, are quite correct. The precision needed by current surface potential based models, however, is far higher. Therefore, a phrase for rectification$u_s = u_{s1} + h$is included in order to achieve the necessary precision, as previously stated. The tiny value of h here corresponds to the surface potential, which is calculated using the second-order correction term of Newton-Raphson. With reference to (19), we may deduce that

$$f(u_s) = U_{GFB} - u_s + q_{an} - q_n - \gamma_1\sqrt{u_s} = 0. \qquad (31)$$

The value of "h"is calculated by referring to equations (31) and (33) from [16]. While assessing the rectification step, eight subbands were taken into accountq_n, q_{an}in addition to its variations. Comparing the analytical value of the surface potential with the numerical findings of (19) confirms the correctness of considering eight subbands, and it reveals that the error is on the order of pV when the corrective process is performed three times.

3. RESULTS AND DISCUSSION

This simplified analytical model matches the reported data obtained by solving the Schrödinger and Poisson equations self-consistently over a wide range of substrate doping concentration and oxide thickness in all regions of

operation very well with respect to the surface potential, accumulation and inversion layer charge densities, and C_G vs V_GB characteristics, taking into account quantum confinement in both the conduction and valence bands.

Figure 2 shows a comparison between the surface potential from this analytical model and the published results [6] from the self-consistent solution of the Schrödinger and Poisson equations. The image clearly shows that the suggested model provides a good fit over a broad range of doping concentrations. The surface potential values in the depletion and inversion regions, as calculated analytically in [16], were unaffected by the incorporation of QM effects in the accumulation region. Consequently, the inversion layer charge and drain current, as shown in Figures 7 and 9 of [16], are identical when calculated using the surface potential values from the proposed model.

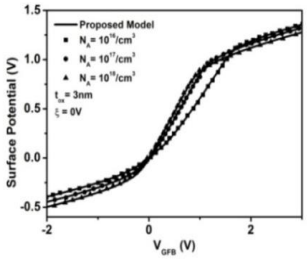

Fig. 2. Comparison of the surface potential obtained from proposed model (solid line) with the reported data [6] obtained by self-consistent solution of Schrödinger and Poisson equations (symbols).

For three distinct doping concentrations with tox = 3 nm, the results obtained from the self-consistent solution of the Schrödinger and Poisson equations [6] and the accumulation layer charge density per unit area obtained using this analytical model correspond quite well (Fig. 3). The self-consistent findings in all three domains of operation demonstrate the validity of the proposed model (Figs. 2 and 3).

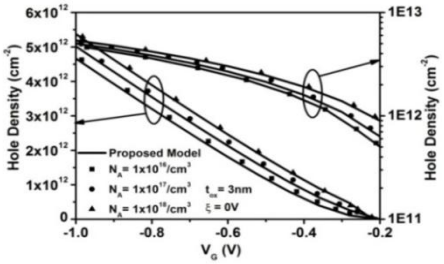

Fig. 3. Comparison of hole density in accumulation layer obtained from proposed model (solid line) with the reported data [6] obtained from self-consistent solution of Schrödinger and Poisson equations (symbols).

Figure 4 displays a comparison of surface potential values derived by several sources, including the suggested analytical model, [8], [34], and the self-consistent solution of the Schrödinger and Poisson equations by Ma et al. [6]. Figure 4 shows that in the inversion and accumulation regions, the findings from [8] differ from [6], and contrary to what is stated in [16], the surface potential is not zero at the flat band. Figure 4 further shows that in the inversion area, the surface potential values from [34] don't match up with the self-consistent findings. It is possible that these differences arise from the fact that in [34] the surface potential values are acquired by applying QM correction on the semi-classical surface potential, while in [8] the QM surface potential is acquired by taking into account just one subband. Surface potential values calculated analytically using the suggested model's triangle potential well approximation with eight subbands, on the other hand, agree extremely well throughout all three operational areas with [6].

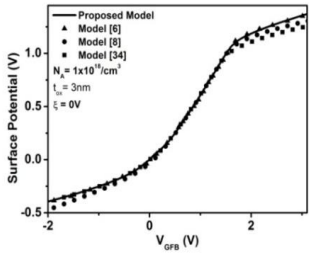

Fig. 4. Comparison of the surface potential values obtained from self-consistent solution of Schrödinger and Poisson equations [6] with reported data [8], [34] and the proposed model.

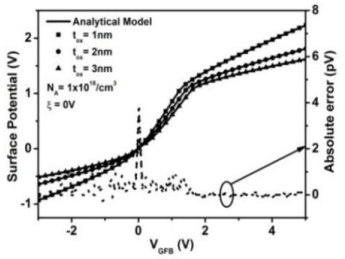

Fig. 5. Comparison of the surface potential obtained from analytical approximation (solid line) with numerical results (symbols) for different values of tox, along with absolute error plot when step-2 is repeated thrice.

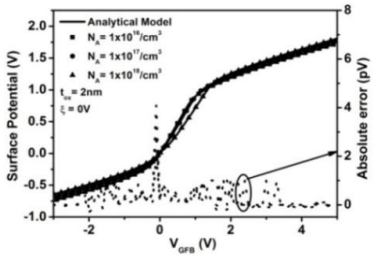

Fig. 6. Comparison of the surface potential obtained from analytical approximation (solid line) with numerical results (symbols) for different values of substrate doping concentration, along with absolute error plot when step-2 is repeated thrice.

For various values of oxide thickness, doping concentration, Figures 5, 6, and 7 show the comparison between the surface potential values calculated using the proposed model and the numerical data derived from (19). For a large variety of device settings, we find that the analytical model's predictions agree well with numerical predictions over all three continuous operating areas. In the area where the accumulation to depletion transition occurs, the absolute error between analytical and numerical findings is around 4 pV; however, in other places, the error is less, as seen in the figures, when step-2 is performed three times. But when step-2 was done again, the inaccuracy was around 2 nV, and it didn't change regardless of the doping concentration, oxide thickness, or □. This demonstrates that the suggested model is correct according to the numerical findings and that the error converges quickly using the Newton Raphson approach.

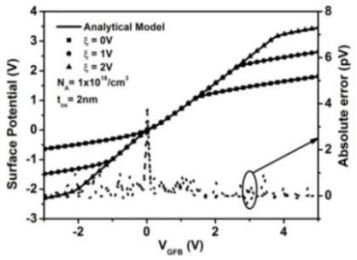

Fig. 7. Comparison of surface potential obtained from the analytical approximation (solid line) with numerically obtained results (symbols) for different values of ξ, along with absolute error plot when step-2 is repeated thrice.

The suitability of proposed analytical model in the compact modeling perspective is further demonstrated by comparing the C_G vs V_{GB} characteristics obtained from the proposed model with the published results, obtained from the self-consistent solution of Schrödinger and Poisson equations, for metal/SiO2/p-Si gate structure [6] as in Fig. 8. We see from the figure, that there is an excellent agreement between the proposed model and the published results from accumulation to inversion region of operation [6]. Whereas results obtained from [16] overestimates capacitance values in accumulation region, since QM effects are not accounted.

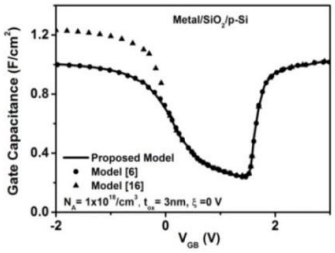

Fig. 8. Comparison of gate capacitance obtained from the proposed model (solid line) with the reported data (symbols) for metal/SiO2/p-Si semiconductor [6], [16].

Figure 9 displays a comparison between the analytical model's third and fourth order derivatives of the surface potential and the findings from the numerical solution of (19), with regard to V_GFB. From the graph, it is clear that the derivatives are smooth and continuous. This guarantees that the surface potential, which takes into account QM effects in the conduction and valence bands, is continuous from the accumulation region to the strong inversion region, even with a fourth-order derivative, and does not show any discontinuity. Therefore, compact models based on surface potential are the best fit for the suggested model.

Figure 10 displays a comparison of the subthreshold current measured from the MEDICI device simulator with data published elsewhere [41] and surface potential values calculated using the suggested model for two distinct drain voltage values. These surface potential values were calculated at the source using quantum mechanics(ψ_{s0})and drain (ψ_{sL})In order to determine the drain current, which is applicable across all operational areas, the suggested model is used in the quantum charge sheet model (7) of [17]. The Id vs Vd curve for the above-threshold region of operation, as shown in Fig. 9 of [16], is applicable to both the proposed model and the published paper. This is because the surface potential values used to find the Id vs Vd curve in both cases are identical.

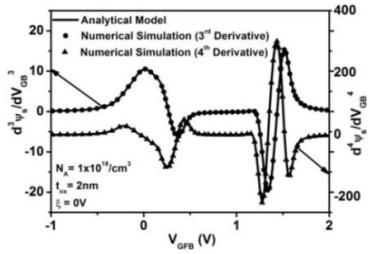

Fig. 9. Third and fourth derivative of the surface potential with respect to VGFBobtained from analytical approximation (solid line) and numerical simulation (symbols).

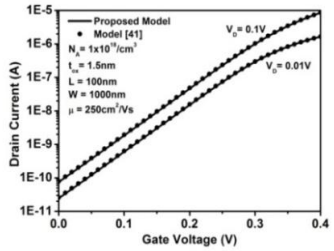

Fig. 10. Comparison of drain current in the subthreshold region obtained from proposed model (solid line) with the reported data [41] (symbols) for two values of drain voltages.

4. Conclusion

An analytical model for surface potential that is based on physics and provides continuity from the accumulation to the strong inversion zone of nMOSFETs is introduced. This model takes into account QM effects in both the accumulation and inversion regions of operation. Without resorting to any corrective procedure, the model incorporates QM effects intrinsically via the use of the triangular potential well approximation. Furthermore, no fitting parameters nor smoothing functions are included in the model. For a large variety of doping densities and oxide thicknesses, the model's surface potential, charge densities, and C_G versus V_GB features agree well with the self-consistent solution of the Schrödinger and Poisson equations. Drain current and derivatives of surface potential shown from a compact modelling viewpoint confirm the model's appropriateness and smoothness. Because it incorporates QM effects intrinsically in both the conduction and valence bands, the simplified analytical model is beneficial for building compact models suited for circuit simulators based on physics. Applying this concept of analytical modelling to multiple-gate MOSFET devices is as simple as decoupling the Schrödinger and Poisson equations, modelling the electrical confinement as a perturbation to the geometrically confined subband energies, and then using the energy band diagram to express the charge density and quasi Fermi potential in terms of surface potential and other physical parameters.

REFERENCES

1. F. Stern and W. E. Howard, “Properties of semiconductor surface inversion layer in the electric quantum limit,” *Phys. Rev.*, vol. 163, no. 3, pp. 816–835, Nov. 1967. DOI: 10.1103/PhysRev.163.816.
2. F. Stern, “Self-consistent results for n-type Si inversion layers,” *Phys. Rev. B, Condens. Matter*, vol. 5, no. 12, pp. 4891–4899, Jun. 1972. DOI: 10.1103/PhysRevB.5.4891.
3. J. A. Pals, “Experimental verification of the surface quantization of an n-type inversion layer of silicon at 300 and 77 ˚K,” *Phys. Rev. B, Condens. Matter*, vol. 5, no. 10, pp. 4208–4210, May 1972. DOI: 10.1103/PhysRevB.5.4208.
4. F. Stern, “Quantum properties of surface space-charge layers,” *CRC Critical Review in Solid State Material Sciences,* vol. 4, pp. 499-514, May 1974. DOI: 10.1080/10408437308245840.
5. J. A. Pals, “Quantization effects in semiconductor inversion and accumulation layers,” *Ph.D. dissertation, Tech. University of Eindhoven, also Philips Res. Reps., suppl.,* vol. 7, pp. 1-84, Jan. 1972. DOI: 10.6100/IR126747.

6. Y. Ma, L. Liu, Z. Yu, and Z. Li, “Validity and applicability of triangular potential well approximation in modeling of MOS structure inversion and accumulation layers,” *IEEE Trans. Electron Devices*, vol. 47, no. 9, pp. 1764–1767, Sep. 2000. DOI: 10.1109/16.861589.
7. R. van Langevelde, A. J. Scholten, and D. B. M. Klaassen, “Physical background of MOS model 11,” *Koninklijke Philips Electron., Amsterdam, The Netherlands,* Apr. 2003.
8. F. Pregaldiny, C. Lallement, and D. Mathiot, “Accounting for quantum mechanical effects from accumulation to inversion, in a fully analytical surface-potential-based MOSFET model,” *Solid State Electron.*, vol. 48, no. 5, pp. 781–787, May 2004. DOI: 10.1016/j.sse.2003.12.010.
9. E. De Castro and P. Olivo, “Quantum effects in accumulation layers on Si-SiO2 interfaces in the WKB effective mass approximation,” *Phys. Status Solidi (b),*vol. 132, pp. 153-163, 1985. DOI: 10.1002/pssb.2221320116.
10. M. I. Vexler, “A simple quantum model for the MOS structure in accumulation mode,” *Solid State Electron.,* vol. 47, pp. 1283–1287, Jan. 2003. DOI: 10.1016/S0038-1101(03)00062-5.
11. A. A. Frantsuzov, S. A. Okhonin, and A. P. Pogosov, “The influence of quantization on the space-charge layer capacitance of Si in strong accumulation,” *Phys. Stat. Sol. (b),*vol. 136, pp. 241–249, 1986. DOI: 10.1002/pssb.2221360127.
12. Y. Ohkura. “Quantum effects in Si n-MOS inversion layer at high substrate concentration,” *Solid State Electron.,*vol. 33, no. 12, pp. 1581-1585, 1990. DOI: 10.1016/0038-1101(90)90138-5.
13. T. Janik and B. Majkusiak, “Analysis of the MOS transistor based on the self-consistent solution to the Schrödinger and Poisson equations and on the local mobility model,” *IEEE Trans. Electron Devices*, vol. 45, no. 6, pp. 1263–1271, Jun. 1998. DOI: 10.1109/16.678531.
14. Y. Ma, L. Liu, W. Deng, L. Tian, Z. Li, and Z. Yu, “A new charge model including quantum mechanical effects in MOS structure inversion layer,” *Solid State Electron.,* vol. 44, pp. 1697–702, 2000. DOI: 10.1016/S0038-1101(00)00090-3.
15. G. Gildenblat, H. Wang, T. L. Chen, X. Gu, and X. Cai, “SP: An advanced surface-potential-based compact MOSFET model,” *IEEE J. Solid-State Circuits,* vol. 39, no. 9, pp. 1394–1406, Sep. 2004. DOI: 10.1109/JSSC.2004.831604.
16. Jayadeva G. S. and DasGupta A., “Analytical approximation for the surface potential in n-channel MOSFETs considering quantum mechanical effects,” *IEEE Trans. Electron Dev.,* vol. 57, no. 8, pp. 1820-1828, Aug. 2010. DOI: 10.1109/TED.2010.20509.
17. B. K. Ip and J. R. Brews, “Quantum effects upon drain current in a biased MOSFET,” *IEEE Trans. Electron Devices,* vol. 45, no. 10, pp. 2213-2221, Oct. 1998. DOI: 10.1109/16.725256.
18. Jordi Sune, Piero Olivo, and Bruno Ricco, “Self consistent solution of the Poisson and Schrödinger equations in accumulated semiconductor insulator interfaces,” *J. Appl. Phys.*, vol. 70, no. 1, pp. 337-345, Jul. 1991. DOI: 10.1063/1.350278.
19. Jordi Sune, Piero Olivo, and Bruno Ricco, “Quantum-mechanical modeling of accumulation layers in MOS structure,” *IEEE Trans. Electron Devices*, vol. 39, no. 7, pp. 1732-1739, Jul. 1992. DOI: 10.1109/16.141240.
20. Scott A. Hareland, M. Manassian, Wei-Kai Shih, S. Jallepalli, Haihong Wang, Gowri L. Chindalore, Al F. Tasch, and Christine M. Maziar, “Computationally efficient models for quantization effects in MOS electron and hole accumulation Layers,” *IEEE Trans. Electron Devices,* vol. 45, no. 7, pp. 1487-1493, Jul. 1998. DOI: 10.1109/16.701479.
21. G. Gildenblat, X. Li, W. Wu, H. Wang, A. Jha, R. van Langevelde, G. Smit, A. Scholten, and D. B. M. Klaassen, “PSP: An advanced surface potential based MOSFET model for circuit simulation,” *IEEE Trans. Electron Devices,* vol. 53, no. 9, pp. 1979–1993, Sep. 2006. DOI: 10.1109/TED.2005.881006.
22. C. B. Duke, “Optical absorption due to space-charge-induced localized states,” *Phys. Rev.*, vol. 159, no. 3, pp. 632-644, Jul. 1967. DOI: 10.1103/PhysRev.159.632.
23. G. A. Baraff and J. A. Appelbaum, “Effect of electric and magnetic fields on the self-consistent potential at the surface of a degenerate semiconductor,” *Phys. Rev. B,* vol. 5, no. 2, pp. 475-497, Jan. 1972. DOI: 10.1103/PhysRevB.5.475.
24. C. Moglestue, “Self consistent calculation of electron and hole inversion charges at silicon–silicon dioxide interfaces,” *J. Appl..Phys.,* vol. 59, pp. 3175-3183, Jan. 1986. DOI: 10.1063/1.336898.
25. Andrea Pacelli, Alessandro S. Spinelli, and Laura M. Perron, “Carrier quantization at flat bands in MOS devices”, *IEEE Trans. Electron Devices,* vol. 46, no. 2, pp. 383-387, Feb. 1999. DOI: 10.1109/16.740906.
26. J. A. Lopez-Villanueva, I. Melchor, F. Gamiz, J. Banqueri, and J. A. Jimenez-Tejada, “A model for the quantized accumulation layer in metal-insulator-semiconductor structures”, *Solid State Electron.,* vol. 38, pp. 203–210, 1995. DOI: 10.1016/0038-1101(94)E0033-B.
27. E. G. Marin, I. M. Tienda-Luna, F. G. Ruiz, J. M. Gonzalez-Medina, A. Godoy, and F. Gamiz, “Analytical potential and charge model of semiconductor quantum wells,” *IEEE Trans. Electron Devices,* vol. 62, no. 12, pp. 4186–4191, Oct. 2015. DOI: 10.1109/TED.2015.2488362.
28. Toan, Ho Le Minh, and Subir Kumar Maity, "Physics based compact modeling of symmetric double gate MOS transistors with high mobility III-V channel material." *Superlattices and Microstructures,* vol. 155, pp. 106925, Jul. 2021. DOI: 10.1016/j.spmi.2021.106925.
29. Menokey, M. Anuja, and Arvind Ajoy, "Airy function based model for 2-DEG charge and surface potential in N-polar Gallium Nitride heterostructures." *IEEE Trans. Electron Dev.,* vol. 69, no. 7, pp. 3861-3868, May 2022. DOI: 10.1109/TED.2022.3175672.

30. Shin, Y. H., Bae, M. S., Park, C., Park, J. W., Park, H., Lee, Y. J., & Yun, I, "Universal core model for multiple-gate field-effect transistors with short channel and quantum mechanical effects." *Semicond. Sci. Technol.,* vol. 33, no. 6, pp. 065010, May 2018. DOI: 10.1088/1361-6641/aac063.
31. R. Rios, N. D. Arora, C. Huang, N. Khalil, J. Faricelli, and L. Gruber, "A physical compact MOSFET model, including quantum mechanical effects, for statistical circuit design applications," in*IEDM Tech. Dig.,*1995, pp. 937–940. DOI: 10.1109/IEDM.1995.499370.
32. G. Gildenblat, T. L. Chen, and P. Bendix, "Closed-form approximation for the perturbation of MOSFET surface potential by quantum-mechanical effects," *Electron. Lett.,*vol. 36, no. 12, pp. 1072–1073, Jun. 2000. DOI: 10.1049/el_20000778.
33. F. Pregaldiny, C. Lallement, R. van Langevelde, and D. Mathiot, "An advanced explicit surface potential model physically accounting for the quantization effects in deep-submicron MOSFETs," *Solid State Electron.,*vol. 48, no. 3, pp. 427–435, Mar. 2004. DOI: 10.1016/j.sse.2003.09.005.
34. M. A. Karim and Anisul Haque, "A physically based accurate model for quantum mechanical correction to the surface potential of nanoscaleMOSFETs," *IEEE Trans. Electron Devices,*vol. 57, no. 2, pp. 496-502, Feb. 2010. DOI: 10.1109/TED.2009.2037453.
35. HISIM. [Online]. Available: https://www.hisim.hiroshima-u.ac.jp/cgi/HiSIM2/public_release.cgi
36. M. J. van Dort, P. H. Woerlee, and A. J. Walker, "A simple model for quantisation effects in heavily-doped silicon MOSFETs at inversion conditions," *Solid State Electron.,*vol. 37, no. 3, pp. 411–414, Mar. 1994. DOI: 10.1016/0038-1101(94)90005-1.
37. [37]T. Ando, A. B. Fowler, and F. Stern, "Electronic properties of two dimensional systems," *Rev. Mod. Phys.*, vol. 54, no. 2, pp. 437–672, Apr. 1982. DOI: 10.1103/RevModPhys.54.437.
38. W. Wu, T.-L. Chen, G. Gildenblat, and C. C. Mc-Andrew, "Physics-based mathematical conditioning of the MOSFET surface potential equation," *IEEE Trans. Electron Devices,*vol. 51, no. 7, pp. 1196–1200, Jul. 2004. DOI: 10.1109/TED.2004.829902.
39. A. R. Boothroyd, S. W. Tarasewicz, and C. Slaby, "MISNAN—A physically based continuous MOSFET model for CAD applications," *IEEE Trans. Comput.-Aided Design Integr. Circuits Syst.,*vol. 10, no. 12, pp. 1512–1529, Dec. 1991. DOI: 10.1109/43.103501.
40. R. Rios, S. Mudanai, W. K. Shih, and P. Packan, "An efficient surface potential solution algorithm for compact MOSFET models," in *IEDM Tech. Dig.,*2004, pp. 755–758. DOI: 10.1109/IEDM.2004.1419282.
41. Jayadeva G. S. and DasGupta A.,"Compact model of short channel MOSFETs considering quantum mechanical effects," *Solid State Electron.,*vol. 53, pp. 649 – 657, May 2009. DOI: 10.1016/j.sse.2009.03.020.